Matthew D. Parker[1]
Auckland Bioengineering Institute,
The University of Auckland,
Private Bag 92019,
Auckland 1142, New Zealand
e-mail: mpar145@aucklanduni.ac.nz

Lynette A. Jones
BioInstrumentation Laboratory,
Massachusetts Institute of Technology,
77 Massachusetts Avenue,
Cambridge, MA 02139
e-mail: ljones@mit.edu

Ian W. Hunter
BioInstrumentation Laboratory,
Massachusetts Institute of Technology,
77 Massachusetts Avenue,
Cambridge, MA 02139
e-mail: ihunter@mit.edu

A. J. Taberner
Department of Engineering Science,
Auckland Bioengineering Institute,
The University of Auckland,
Private Bag 92019,
Auckland 1142, New Zealand
e-mail: a.taberner@auckland.ac.nz

M. P. Nash
Department of Engineering Science,
Auckland Bioengineering Institute,
The University of Auckland,
Private Bag 92019,
Auckland 1142, New Zealand
e-mail: martyn.nash@auckland.ac.nz

P. M. F. Nielsen
Department of Engineering Science,
Auckland Bioengineering Institute,
The University of Auckland,
Private Bag 92019,
Auckland 1142, New Zealand
e-mail: p.nielsen@auckland.ac.nz

Multidirectional In Vivo Characterization of Skin Using Wiener Nonlinear Stochastic System Identification Techniques

A triaxial force-sensitive microrobot was developed to dynamically perturb skin in multiple deformation modes, in vivo. Wiener static nonlinear identification was used to extract the linear dynamics and static nonlinearity of the force–displacement behavior of skin. Stochastic input forces were applied to the volar forearm and thenar eminence of the hand, producing probe tip perturbations in indentation and tangential extension. Wiener static nonlinear approaches reproduced the resulting displacements with variances accounted for (VAF) ranging 94–97%, indicating a good fit to the data. These approaches provided VAF improvements of 0.1–3.4% over linear models. Thenar eminence stiffness measures were approximately twice those measured on the forearm. Damping was shown to be significantly higher on the palm, whereas the perturbed mass typically was lower. Coefficients of variation (CVs) for nonlinear parameters were assessed within and across individuals. Individual CVs ranged from 2% to 11% for indentation and from 2% to 19% for extension. Stochastic perturbations with incrementally increasing mean amplitudes were applied to the same test areas. Differences between full-scale and incremental reduced-scale perturbations were investigated. Different incremental preloading schemes were investigated. However, no significant difference in parameters was found between different incremental preloading schemes. Incremental schemes provided depth-dependent estimates of stiffness and damping, ranging from 300 N/m and 2 Ns/m, respectively, at the surface to 5 kN/m and 50 Ns/m at greater depths. The device and techniques used in this research have potential applications in areas, such as evaluating skincare products, assessing skin hydration, or analyzing wound healing. [DOI: 10.1115/1.4034993]

Keywords: indentation, in vivo skin mechanics, linear dynamics, multidirectional indentation, static nonlinearity, Wiener cascade

Introduction

Changes in skin properties occur as a consequence of many variables, including localized and systemic diseases, ageing, UV damage, and the use of skincare products. Dermatological health traditionally has been assessed qualitatively, through visual examination and touch. Qualitative methods provide limited insight into the anisotropic, heterogeneous, viscoelastic, and nonlinear mechanical properties of skin. Research devices that provide quantitative measures of the skin's mechanical properties allow more reliable evaluation of its health and provide a more standardized method of assessment than visual or tactile examination. However, such devices have yet to achieve significant use in clinical environments. A single device that can perform high bandwidth, three-dimensional, large-scale deformations could improve the assessment of treatment regimens and skincare products, diagnosis of skin and systemic conditions, and help provide an understanding of the mechanics associated with artificial skin development.

Current research devices and clinical products for in vivo skin assessment typically employ a single mode or method of deformation, such as suction [1–5], torsion [6,7], indentometry [8–11], ballistometry [12], shear deformation [13–15], or extensometry [16–18]. Mechanical properties reported using these techniques vary widely. Values for simple parameters, such as the Young's modulus, have varied by over 3 orders of magnitude [19]. Variations in such estimates may arise from the choice of spatial and frequency ranges over which the skin is perturbed. More elaborate phenomenologically or structurally based models can capture the complex mechanical behavior more accurately, but are difficult to interpret clinically. Many testing protocols involving skin deformation are performed using relatively small displacements that are intended to correspond to the normal physiological range. Such techniques may produce a locally linear response. However, larger-scale displacements performed at the same location can give rise to strikingly different estimates of material parameters.

[1]Corresponding author.
Manuscript received May 24, 2016; final manuscript received October 7, 2016; published online November 4, 2016. Assoc. Editor: Kristen Billiar.

By perturbing the skin using higher strains, useful information may be revealed about its structure or underlying constituents which may be relevant in applications such as adjusting the penetration depth of a needle-free jet injection. The estimates of skin properties can be affected by the level of preload on the skin, which can place the local perturbations at an unknown location along the full-scale force–displacement curve. In addition, very few deformation devices have attempted to characterize the dynamic properties of skin [20–25], with the majority opting to minimize viscous effects by perturbing at quasi-static rates. A device that can perturb skin throughout its nonlinear stress–strain curve, at varying rates, may provide the basis for standardized testing of skin.

Single modes of deformation fail to determine the anisotropic skin response in directions both planar and normal to the skin surface [26]. Chen and Hunter [24,25,27] and Sandford et al. [20] fabricated a dynamic indenter that could be repositioned on the skin surface to record both normal indentation and tangential extension deformations over large displacements. The device consists of a voice-coil style Lorentz-force motor that perturbs a probe at high bandwidth while it is held in contact with the skin surface. The motor's force output is measured through a current sensing resistor, and the tip position is recorded with a linear potentiometer attached to the motor. Characterization of the dynamic response of skin is performed using stochastic system identification techniques, which permit perturbations with multiple frequency components to be applied simultaneously. Frequency-rich stochastic signals reduce the test duration when compared to other dynamic protocols, such as swept sinusoid approaches. This benefits both subjects and clinicians and reduces errors due to subject motion that is often problematic. Models of the system's responses, such as a Wiener system or Volterra kernels, describe the linear dynamics and static nonlinearity of skin and provide measures of the stiffness, damping, and perturbed mass of the bulk material.

The device used by Chen and Hunter and Sandford et al. requires repositioning on the skin if both normal and tangential deformations are implemented. However, relocating the probe tip introduces measurement delay between deformation modes and some positioning uncertainty at the skin site, which may lead to errors in the resulting parameterization of the skin's response. Errors due to relocation can be avoided if the system does not require reconfiguration of the testing device. A microrobotic device capable of performing both normal and tangential deformations has been described by Flynn et al. [28]. Similar to the device developed by Chen and Hunter, dynamic force inputs are provided via voice-coil actuators. A novel feature of the microrobot is that it uses three voice coils arranged in parallel to move a probe tip through an approximately spherical working volume. The location of the probe tip is reconstructed from the kinematics of the individual motor positions, which are quantified using linear potentiometers.

In this paper, we describe the use of this multiaxis microrobot to dynamically perturb the skin in multiple directions without repositioning the probe tip. Indentation and extension tests were conducted on the thenar eminence of the hand (at the base of the thumb) and on the volar forearm. These areas of markedly different mechanical properties were chosen to test the experimental feasibility of the device. Extensive literature can be found on the dynamic mechanical properties of the hairy skin on the forearm, but relatively little research exists on the glabrous skin of the thenar eminence.

The present work uses linear and Wiener stochastic system identification techniques, combined with a versatile microrobotic instrument, to characterize the anisotropic properties of skin on the volar forearm and thenar eminence. With the use of these tools, measures of the bulk properties of skin and underlying tissue can be obtained, including the high-frequency dynamics and static nonlinearities in both glabrous and hairy skin. The short experiments (5 s each) are shown to yield accurate results in both indentation and extension. Although setup time was not measured, we estimate a setup time of approximately 5 min. The procedure is robust and lends itself well to automation. The application of perturbation protocols, data processing, and parameter estimation can be performed in a single operator step, which could provide a rapid and simple use of clinical tool. A study of the difference between full-scale and incremental loading schemes, and the effect of preconditioning routines for system identification is also presented.

Materials and Methods

Experimental Apparatus. A three-axis microrobot, similar to that of Flynn et al. [28] shown in Fig. 1, underwent modifications to its force transduction and timing hardware so that stochastic system identification techniques could be implemented to characterize the dynamic mechanical properties of human skin. Briefly, the robot consists of three Lorentz-force actuators (LA-10-12-027 A, BEI-Kimco, Vista, CA) arranged in parallel, each attached to a vertex of a triangular moving platform. Atop the moving platform is an interchangeable digital ABS (Stratasys Ltd., Eden Prairie, MN) printed cylindrical probe tip 4 mm in diameter. Linear potentiometers on each actuator allow 3D resolution of the probe tip location.

The stochastic system identification technique that has been employed in this work relates the motor force to the position of the probe. The force generated by a voice-coil motor is linearly

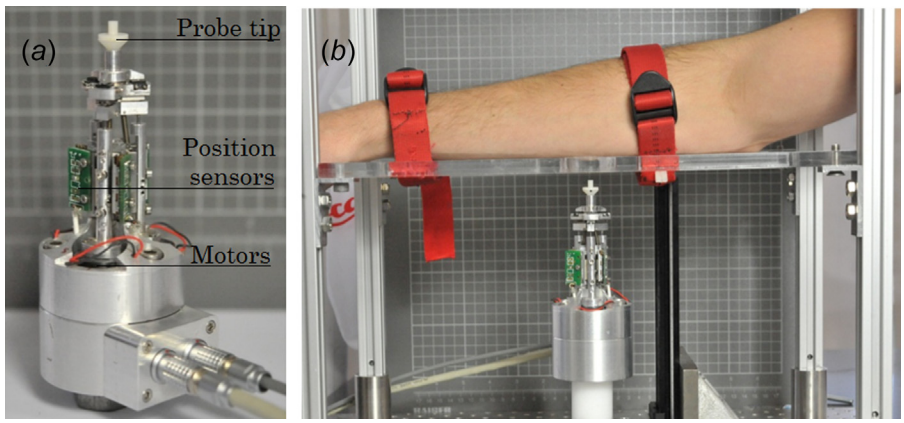

Fig. 1 Microrobot device used to perturb skin in vivo. (*a*) A close-up of the robot components. (*b*) A potential skin site positioned on the aluminum-acrylic support structure prior to testing. Note that the relative positions of the robot and subject's arm are chosen for demonstrative purposes and do not reflect exact test conditions presented in this study.

proportional to the current passing through it. In this iteration of the microrobot, the motor current was measured from the voltage developed across a 0.4 Ω current-sense resistor placed in series with each motor.

The robot tip has a maximum vertical and horizontal travel of 9 mm and 50 mm, respectively. The maximum stroke of the robot is smaller than that of the device described by Chen and Hunter [27], but large enough to perturb the epidermis, dermis, and hypodermis in areas of skin with low body fat, such as the forearm, face, and palm.

Stochastic System Identification Hardware. Dynamic system identification requires a deterministic control and measurement environment. Modifications to the device described by Flynn et al. [9,28,29] included moving the timing control from the Microsoft Windows environment to LABVIEW 2011 REALTIME software (National Instruments, Austin, TX). Microrobot control signals and measurements were made on a compactRIO FPGA-based system (cRIO-9022 and cRIO-9114, National Instruments) running LABVIEW 2011 REALTIME software. Data acquisition and motor control were performed at a rate of 2 kHz.

A voltage signal was generated for the three motor axes, using a 16-bit analog output module (NI 9264, National Instruments). The signals were amplified by a custom amplifier board, housing a separate linear amplifier (PA 74, Apex Microtechnologies, Tucson, AZ) for each axis. The force constant versus position of each Lorentz-force actuator was measured using a force–torque transducer (Nano17, ATI Industrial Automation, Apex, NC). Signals from the current and position sensors were acquired through a 16-bit analog input module (NI 9205, National Instruments).

An overview of the system architecture is presented in Fig. 2. The input to the system is a voltage signal, generated offline, and executed by the analog output module during the experiment. The voltage is passed through the linear amplifier(s) to the Lorentz-force actuator(s) generating the force(s) $F^*(t)$ that, in turn, perturbs the probe on the skin at position $P^*(t)$. The current $I^*(t)$ delivered to the Lorentz-force actuators is measured by current-sense resistors, resulting in the force measurements $x(t)$, with associated error $e_1(t)$. Likewise, potentiometer estimates of position $y(t)$ contain error $e_2(t)$. Note that this schematic applies for both normal indentation and tangential extension.

Stochastic System Identification. Skin and its underlying tissue structures form a nonlinear dynamic system. Like many biological systems, skin can be modeled as the combination of a linear dynamic system and a static nonlinearity. Wiener cascade models have been shown to provide a good description of the response of skin, where a static nonlinearity follows a linear dynamic component [25]. Note that the reverse order, where the linear dynamics cascade on from the static nonlinearity, represents a Hammerstein system which does not capture skin behavior as effectively [24].

In a linear dynamic system, the impulse response function (IRF) provides a linear map of the input to the output. Identification of the impulse response function requires the biased cross-correlation of a stochastic input signal with the resulting output signal, as well as the biased autocorrelation of the input signal. A detailed description of the method is presented in Chen and Hunter [25]. For brevity, the impulse response function (IRF) is calculated in the following equation:

$$\mathrm{IRF} = F_s(R^{-1}\varnothing_{xy}) \tag{1}$$

where $\varnothing_{xy}$ is the cross-correlation of the input x and output y, and R is the Toeplitz matrix of the autocorrelation function, sampled at frequency F_s. Singular value decomposition was chosen to invert the Toeplitz matrix in order to avoid possible numerical instabilities seen in many other inversion methods. The resulting impulse response function is second order and can be represented by a damped sinusoid. Parameterization of the damped sinusoid was performed using a Levenberg–Marquardt nonlinear optimization. The parameters of the damped sinusoid can then be converted into mass, stiffness, and damping terms [20]. Optimization of the sinusoid parameters allowed comparisons between the variance accounted for (VAF) by the nonparametric model and by the subsequent parametric model.

The output of a truly linear system can be recreated by convolving the input signal with the impulse response function. As skin is nonlinear, its IRF cannot completely account for the variance in the output signal. The variance accounted for by the impulse response has been shown to increase when passing the linear-predicted output through a static nonlinearity [27]. A static scaling term can be moved between the linear dynamics and static nonlinearity. The DC compliance (mm/N) was chosen as the constant by which the linear impulse response function was divided; doing so produced a predicted linear output in Newton. By comparing the output predicted by the linear impulse response with the measured output, a polynomial describing the disparity may be found. The inverse function is then applied to the linear IRF, creating a new, nonlinear estimate. This last step is iterated until the variance accounted for converges. The form of the nonlinearity is described in the following equation:

$$Y = C_1(1 - e^{-C_2 x}) \tag{2}$$

where C_1 is a measure of the total compressible thickness of the perturbed tissue, and C_2 determines how the bulk material's stiffness is affected as the indenter goes further into the skin. Note

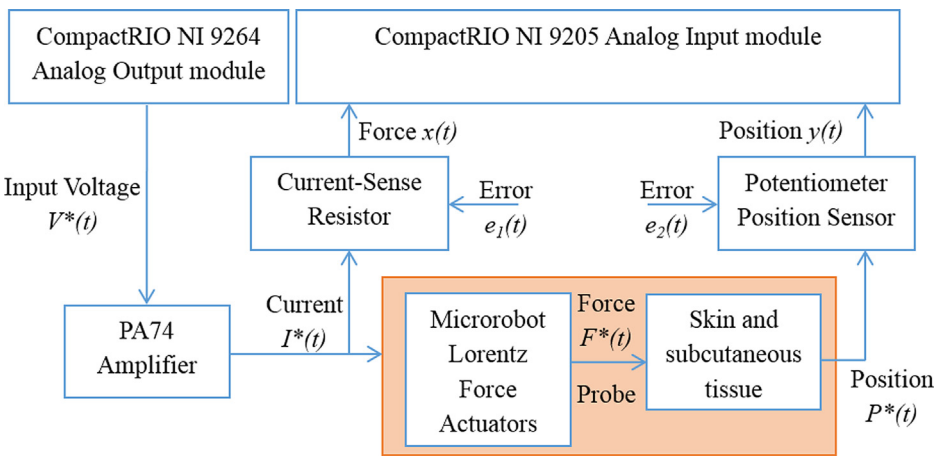

Fig. 2 Schematic system diagram. The system refers exclusively to the combination of the robot and tissue.

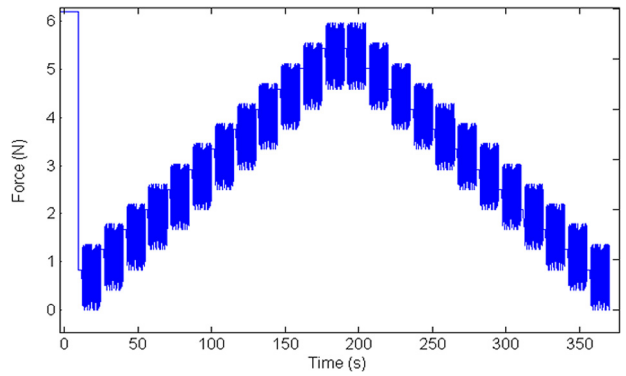

Fig. 3 Stochastic input with stepwise increase in mean, referred to as "protocol B." Preconditioning at each step was performed by holding the mean value. The first 10 s show a full-scale preconditioning step where the maximum output force is held for demonstrative purposes and do not reflect exact test conditions presented in this study.

that, when incorporating the nonlinearity, the system is reduced from three to two degrees-of-freedom. When the impulse response function is divided by the DC compliance it folds the spring contribution into C_1 and C_2, giving rise to scaled mass M_s and scaled damping B_s parameters.

Stochastic Signal Inputs. A stochastic force profile was generated offline in LABVIEW. The profile was scalable to produce up to 3.5 N force per motor, with a Gaussian probability distribution. The resulting signal was low-pass filtered at 200 Hz, as frequency components above this limit are likely to exceed the bandwidth limit of the system and/or cause pain [25]. Under normal indentation, forces up to 10.5 N could be applied, as the force produced by each motor was summed. Three approximately tangential surface extension directions could be defined by passing the stochastic input through a single motor, while providing sufficient current to lock the remaining motors in their base positions. Three force input protocols were created for skin characterization: a full-scale input and two incremental inputs. Incremental inputs were created by scaling the full-scale input to 20% and stepping its mean value across the full-scale range. Fifteen increments and decrements were performed sequentially to investigate any hysteresis in the incremental response. The incremental protocols varied by their form of preconditioning before each increment. The first protocol (denoted "protocol A") began each increment with a zero-maximum-zero force triangle wave, while the second protocol ("protocol B" and shown in Fig. 3) held the mean input value from the subsequent increment. Overall preconditioning of the skin was performed by applying a 0.5 Hz sinusoidal ramp from zero to full force output for three periods, followed by 10 s at the maximum input force, and then applying the stochastic signal for 100 s at full force output. Performing this preconditioning routine produced repeatable indentation depths to approximately 20 μm.

Participants. Ten male subjects who ranged in age from 21 yrs to 43 yrs participated in the experiments. They all signed an informed consent form as required by the University of Auckland Ethics Committee.

Experimental Procedure. Tests were conducted in an air-conditioned room, where temperature varied between 23 °C and 24 °C, and relative humidity varied between 44% and 50%.

Full-scale normal indentation and tangential stretches were applied to the left forearm and palm of the subjects. The forearm of each subject was strapped to an acrylic plate, which was suspended by an aluminum frame designed to overhang the microrobot. Subjects were asked to relax their hands so that their fingers were loosely flexed as the hand extended beyond the acrylic plate. The subject's arm was essentially straight, with a natural resting angle of the elbow similar to that illustrated in Fig. 1(*b*). A 40 mm diameter hole in the plate provided access to the skin. Double-sided adhesive tape spanned the hole, isolating the test area from the surrounding skin, thereby limiting the mass of tissue providing the force–displacement response, and minimizing movement at the surface of the skin at the boundary of the hole. Liquid cyanoacrylate was used to attach the probe tip to the skin, in accordance with previous dynamic studies [20,27]. Cyanoacrylate provided a firm bond between the skin and probe tip and securely coupled the skin to the indenter. At the end of the test session, subjects applied tension to the tip to remove it from the skin. When testing the thenar eminence, straps were placed across the wrist and the fingers and thumb, with the fingers extended together across the acrylic plate.

Indentations were made at a position 100 mm from the elbow along the volar surface of the forearm and in the center of the thenar eminence at the base of the thumb of each subject. The total force input was adjusted for each subject so that the response was limited to be within the maximum probe travel. Incremental normal indentation and tangential stretches were also applied to the same locations for five subjects. Each protocol was initiated immediately after the first protocol was completed.

Tangential extension stretches were applied along the surface of the forearm of the subject by actuating a single axis at a time. The same signal was then applied to another axis, stretching the skin at 120 deg relative to the first axis. Finally, the third axis was actuated, generating a stretch in a direction −120 deg relative to the first axis (refer to Fig. 4).

Data Analyses. Two-way repeated measures analysis of variance (ANOVAs) were performed to test whether there was any significant effect of testing site (thenar eminence and forearm) and direction (indentation and extension) or interaction between these two factors for any of the nonlinear parameters calculated. One-way repeated measures ANOVAs were performed to test whether

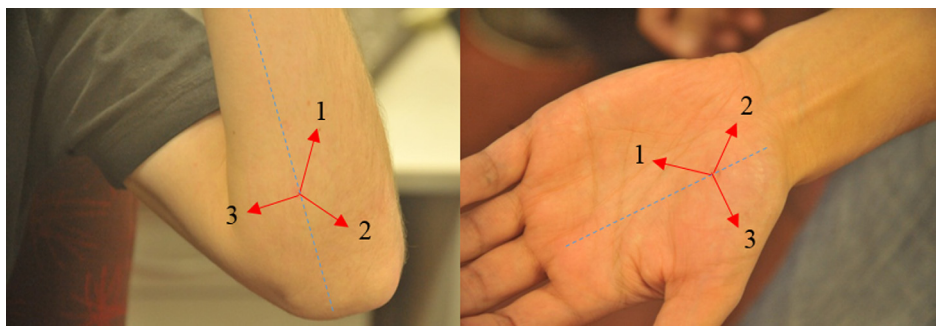

Fig. 4 Location, direction, and order of applied tangential stretches. Dashed line indicates approximate proximal–distal axis that intersects the test site.

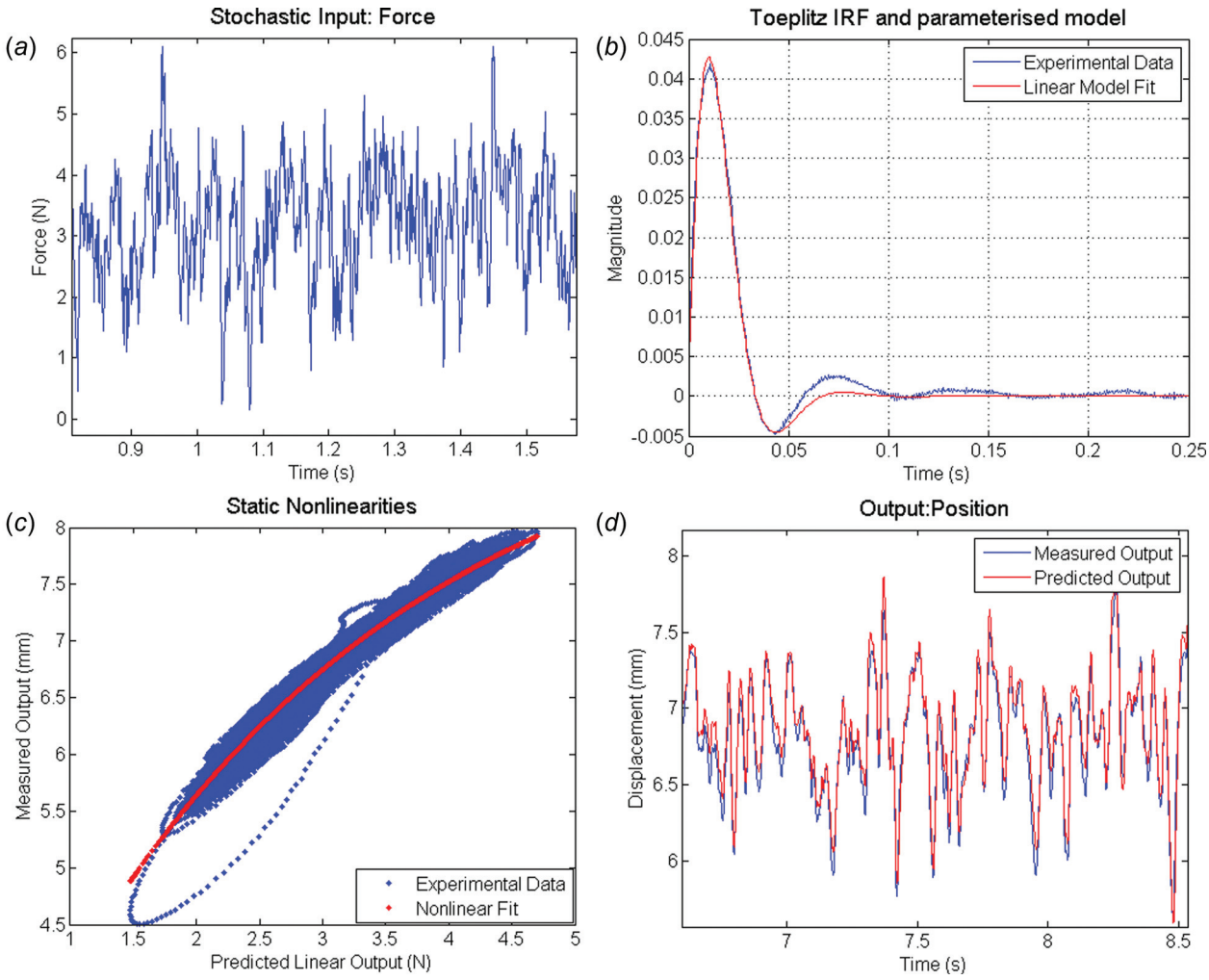

Fig. 5 Representative experimental results from nonlinear stochastic system identification on the volar forearm. The measured input force (*a*) is used to generate the linear impulse response function (*b*), shown blue in measured form and red in parameterized form. The linear dynamics are then passed through the Wiener nonlinearity, as shown in blue in (*c*). The nonlinearity has been parameterized, shown by the red line. The output of the Wiener nonlinearity is shown in (*d*), where the Wiener-predicted output (red) is shown against the potentiometer-measured output (blue).

there was any statistically significant anisotropy in nonlinear parameters calculated from tangential stretches applied to the volar forearm. Due to difficulties in applying tangential stretches on the thenar eminence, its anisotropy could not be assessed.

Coefficients of variation (CVs, i.e., the standard deviation of a parameter divided by its mean) were calculated for parameterized linear and Wiener models of skin. The CV of parameters for a single individual assesses the reliability of the device, whereas the CV of parameters across individuals may provide insights about physiological variability. The CV within individuals is calculated as $(1/N)\sum_{n=1}^{N}(\sigma_n/\mu_n)$, where N is the total number of participants, and σ_n and μ_n are the standard deviation and mean, respectively, for participant n, for a given parameter and test direction. The CV across individuals was calculated as (σ/μ), where σ and μ are the standard deviation and mean, respectively, of every test and every participant, for a given parameter and test direction.

Linear elastic parameters were used to provide estimates of the Young's modulus E for comparison with previous literature. For a semi-infinite body under normal indentation, E can be estimated by

$$E = \frac{(1-\nu^2)K}{2R_p} \tag{3}$$

where ν is the Poisson's ratio, K is the spring contribution, and R_p is the probe radius. Likewise, the parameters for a neo-Hookean model, c_{10} and D_1, can be generated from the Poisson's ratio and the Young's modulus, by

$$c_{10} = \frac{E}{4(1+\nu)},\ D_1 = \frac{6(1-2\nu)}{E} \tag{4}$$

Results

Linear Dynamics and Static Nonlinearities. For each test procedure, a linear prediction of the impulse response function

Table 1 Group mean parameter values and standard deviations for the linear dynamic model

Position/direction	K (kN/m)	M (g)	B (N s/m)	VAF (%)[a]
Forearm/normal	1.45 ± 0.21	15.5 ± 7.1	4.76 ± 1.8	93.4 ± 2.1
Palm/normal	2.75 ± 1.04	6.40 ± 3.0	8.27 ± 2.0	93.1 ± 1.6
Forearm/1	2.09 ± 0.42	7.81 ± 2.3	2.81 ± 1.24	92.4 ± 4.6
Forearm/2	1.56 ± 0.23	3.72 ± 2.3	2.98 ± 0.66	93.4 ± 2.0
Forearm/3	1.95 ± 0.39	8.40 ± 1.4	2.75 ± 0.65	94.1 ± 3.0
Palm/3	4.00 ± 0.94	4.11 ± 2.0	4.7 ± 1.06	93.7 ± 3.7

Note: Mass (K), perturbed mass (M), damping (B), and variance accounted for (VAF) are displayed for each testing site and mode of deformation.

Table 2 Parameter means and standard deviations of the subjects for the Wiener static nonlinearity model

Position/direction	M_s (s^2)	B_s (s)	C_1 (mm)	C_2 (1/N)	VAF (%)[a]
Forearm/normal	0.0655 ± 0.009	8.94 ± 0.83	8.64 ± 2.00	0.510 ± 0.12	96.7 ± 1.0
Palm/normal	0.0347 ± 0.012	6.52 ± 1.69	8.49 ± 0.85	0.506 ± 0.15	96.5 ± 1.4
Forearm/1	0.0078 ± 0.002	2.86 ± 0.54	1.51 ± 0.39	2.00 ± 1.02	95.2 ± 2.9
Forearm/2	0.0075 ± 0.002	3.38 ± 0.44	1.78 ± 0.28	2.02 ± 0.67	93.5 ± 3.2
Forearm/3	0.0111 ± 0.003	3.17 ± 0.72	1.92 ± 0.42	1.69 ± 0.70	95.8 ± 2.4
Palm/3	0.0044 ± 0.003	2.46 ± 0.72	1.49 ± 0.41	1.34 ± 0.67	94.5 ± 4.1

Table 3 Mean coefficients of variation within and between individuals

	CV MEANS FOR INDIVIDUALS (%)				CV means across individuals (%)			
Position/direction	C_1	C_2	M_S	B_S	C_1	C_2	M_S	B_s
Forearm/normal	4.6	10.1	2.4	3.3	23.1	22.7	14.1	9.3
Palm/normal	3.9	11.2	2.6	3.7	10.0	30.6	35.0	25.9
Forearm/1	9.4	18.3	3.6	3.1	25.6	55.8	30.5	20.5
Forearm/2	9.9	19.3	5.6	3.1	16.2	33.2	26.5	13.0
Forearm/3	11.3	19.5	3.3	2.7	22.1	41.3	24.6	22.9
Palm/3	9.74	12.6	3.1	2.9	27.2	49.7	63.1	29.3

Note: Coefficients of variation (CV) for an individual express repeatability of test results for a single individual. CV for a single individual is calculated as the mean parameter value across test repeats, divided by the standard deviation of the parameter. Each subjects' CV is then averaged to produce the CV mean for individuals. CV means across individuals expresses the variation of parameters within the subject pool. The CV means across individuals uses the mean and standard deviation of every test repeat, over every subject for a given parameter.

was made before the static nonlinearity was fit between the linear-predicted output and the measured output.

Representative results for normal indentation on the volar forearm are shown in Fig. 5. A sample section of the measured stochastic force input is shown in Fig. 5(*a*). Parameterization of the Toeplitz-inverted impulse response function typically showed a qualitatively good fit, but often deviated around the peaks of the sinusoid (as seen in Fig. 5(*b*)). The impulse response function followed a typical underdamped sinusoidal system response, with memory length less than 0.25 s. The static nonlinearity (seen in Fig. 5(*c*)) was found by comparing the measured output with the predicted linear output. A two-parameter curve (see Eq. (2)) was used to describe the nonlinearity. The change in compliance as the tissue is displaced can be assessed by calculating the slope at locations along the curve. In accordance with behavior noted by Chen and Hunter [25], the looping in the experimental data is a physiological phenomenon, likely due to the viscoelasticity of the tissue. The predicted output resulting from the Wiener nonlinearity is compared to the actual output in Fig. 5(*d*), which shows a qualitatively good fit over the length of the protocol, with some deviation seen during large changes in displacement.

Full-Scale Perturbations. Group mean linear estimates of model parameters are presented in Table 1, where they are classified by the location and direction of perturbation. Linear estimates of the microrobot's mass and damping were subtracted from system estimates to produce the bulk tissue parameters listed. Under normal indentation, the volar forearm showed an average stiffness of 1.45 kN/m, while the thenar eminence showed a stiffness of 2.75 kN/m. However, the range of thenar stiffness estimates spanned the upper limit of volar forearm estimates, and two subjects displayed higher stiffness on their forearm relative to their palm. Up to 35 g of tissue mass was perturbed on the forearm, compared to 10 g on the thenar eminence. Damping on the palm

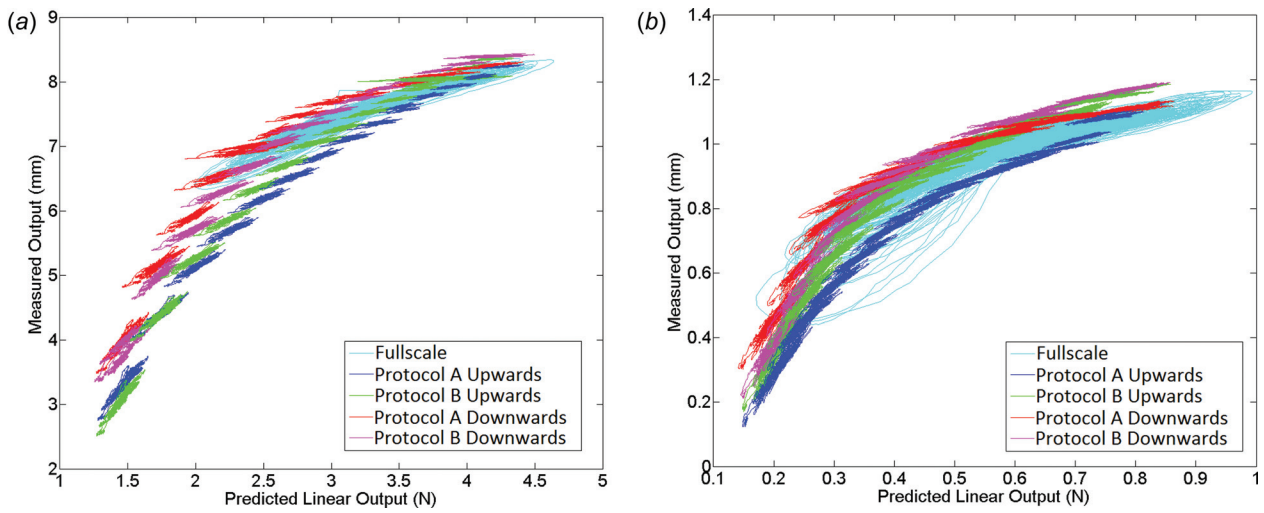

Fig. 6 Representative static nonlinearity plot for a volar forearm using incremental loading schemes, protocols A and B under (*a*) normal indentation and (*b*) extension

was also shown to be approximately double that of the volar forearm.

For extension experiments, the thenar eminence again showed stiffer responses than the volar forearm, with a larger range of stiffness values across subjects. The much smaller tangential responses on the thenar eminence, presumably due to its higher stiffness, were insufficient for system identification. The results could only be obtained from seven subjects in direction 3 on the palm. Significant anisotropy was evident among the different perturbation directions on the forearm. Stiffness measures were lowest in direction 2 (1.5 kPa) (see Fig. 4) and were approximately 2 kPa in directions 1 and 3. Estimates of mass ranged from 4 g to 8 g, depending on the direction of stretch. There was little variation in the average damping across the perturbation directions and sites tested in extension, with values ranging from 2.75 N s/m to 2.98 N s/m on the volar forearm and 4.7 N s/m on the thenar eminence.

Whereas the linear model's variance accounted for was 93.4% for the forearm under normal indentation, Wiener models produced average increases in VAF of 3.3%. For lateral stretches, linear VAF ranged from 92.4% to 93.4%, depending on direction, with Wiener models providing a further 0.1% to 2.8% average increase. Linear models of normal indentation of the thenar eminence had VAF between 87.5% and 94.7%, with Wiener model improvements of 2.6–4.0%. For the remaining thenar eminence extension experiments, linear VAFs averaged 93.7%, with Wiener models increasing the VAF a further 0.8%.

Wiener static nonlinearity parameters are presented in Table 2. The volar forearm shows greater scaled mass and scaled damping than the palm, whereas there is little to distinguish the compressible depth or degree of nonlinearity between the two sites. The anisotropy of forearm extension displayed in the nonlinear model is less apparent. The scaled mass, scaled damping, compressible length, and degree of nonlinearity are similar between directions 1 and 2, whereas direction 3 exhibited slightly higher scaled mass and compressible length, a slightly lower rate of change of stiffness, and a similar scaled damping.

Two-way repeated measures ANOVAs with site (forearm and thenar eminence) and direction (indentation and extension) as factors were conducted on each of the four parameters (C_1, C_2, M_s, and B_s). There was a main effect of site on M_s, ($F(1,6) = 15.862$, $p < 0.01$) and B_s ($F(1,6) = 8.934$, $p = 0.02$), with the forearm having higher scaled mass and damping. There was no effect of site on either M_s or B_s. For all the parameters, there was an significant effect of the direction of testing, with indentation resulting in higher estimates of C_1 ($F(1,6) = 378$, $p < 0.01$), M_s ($F(1,6) = 131.9$, $p < 0.01$), and B_s ($F(1,6) = 180$, $p < 0.01$) and extension resulting in higher estimates of C_2 ($F(1,6) = 49.59$, $p < 0.01$). None of the interactions was significant.

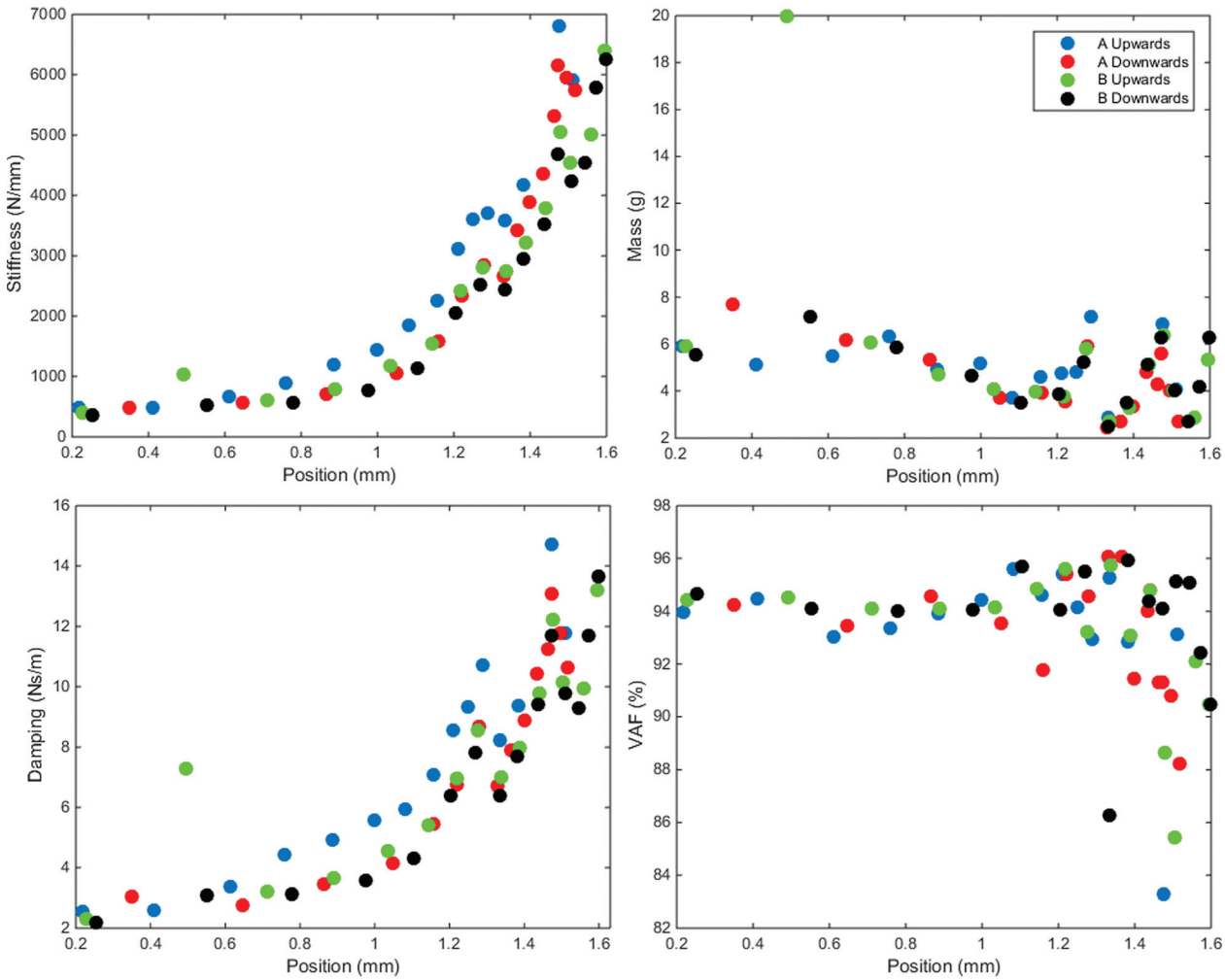

Fig. 7 Representative experimental results from linear stochastic system identification on a forearm using incremental loading, under normal indentation and across-surface extension. (*a*) The tissue stiffness estimated at various stretches is shown. (*b*) The perturbed mass estimated as various stretches is shown, after the actuator mass is subtracted. (*c*) The tissue damping at various stretches is shown after the actuator damping is subtracted. (*d*) The VAF for each site is plotted against actuator tip position.

The results from the one-way repeated measures ANOVAs showed that there was a statistically significant difference between directions for M_s ($F(2,18) = 11.103$, $p = 0.001$) and B_s ($F(2,18) = 9.165$, $p = 0.002$), but no effect on C_1 or C_2. Pairwise comparisons showed significant differences in M_s for all the directions (all the p-values < 0.001) and in B_s for directions 1 and 2 ($p = 0.004$) and 1 and 3 ($p = 0.032$).

The average CVs within individuals and across individuals are listed for the nonlinear parameters in Table 3. Under normal indentation, the CVs within individuals were between 2% and 11%, whereas the range of CVs across individuals was higher (9–37%). Under extension, CVs of the model parameters within individuals varied between 3% and 20% and across individuals ranged from 13% to 63%. Across both sites and perturbation types, M_s and B_s demonstrated the lowest CVs within individuals, which were between 3 and 20 times lower than CVs across individuals.

Incremental Perturbations. Representative experimental results for the perturbation schemes, protocol A and protocol B, applied to the volar forearm under normal indentation and extension are presented in Fig. 6. Both perturbation schemes are separated into ascending and descending parts. The incremental loading curves appear to have flatter slopes than the full-scale loading curves, especially in normal indentation (Fig. 6(*a*)). Hysteresis can be seen in the offsets of the groups, although individual increments showed little difference in gradient across directions or protocols. The difference in offset between the protocols, seen in both panels in Fig. 6, was shown to depend on the order of perturbations. In other words, by performing protocol B before protocol A, the offsets that are displayed in Fig. 6 were reversed, with the results from protocol A located within the loop of protocol B. This behavior suggests that the output displacement is more sensitive to the level of preconditioning than it is to the type of preconditioning. The same general appearance of Fig. 6 is held across perturbation sites and preconditioning levels.

Linear parameter estimates of tissue stiffness, mass, damping, and the VAF for the different incremental protocols are plotted against position for an incremental extension experiment on the forearm in Fig. 7. The reported mass and damping parameters have had the constant estimates of the robot's mass and damping removed. The stiffness and damping parameters show a monotonically increasing trend with increasing stretch of the skin, whereas the mass and VAF remain relatively constant. However, the VAF decreases toward the upper limits of extension.

The linear estimates of stiffness, mass, damping, and VAF are presented for normal indentation of the forearm and palm and an

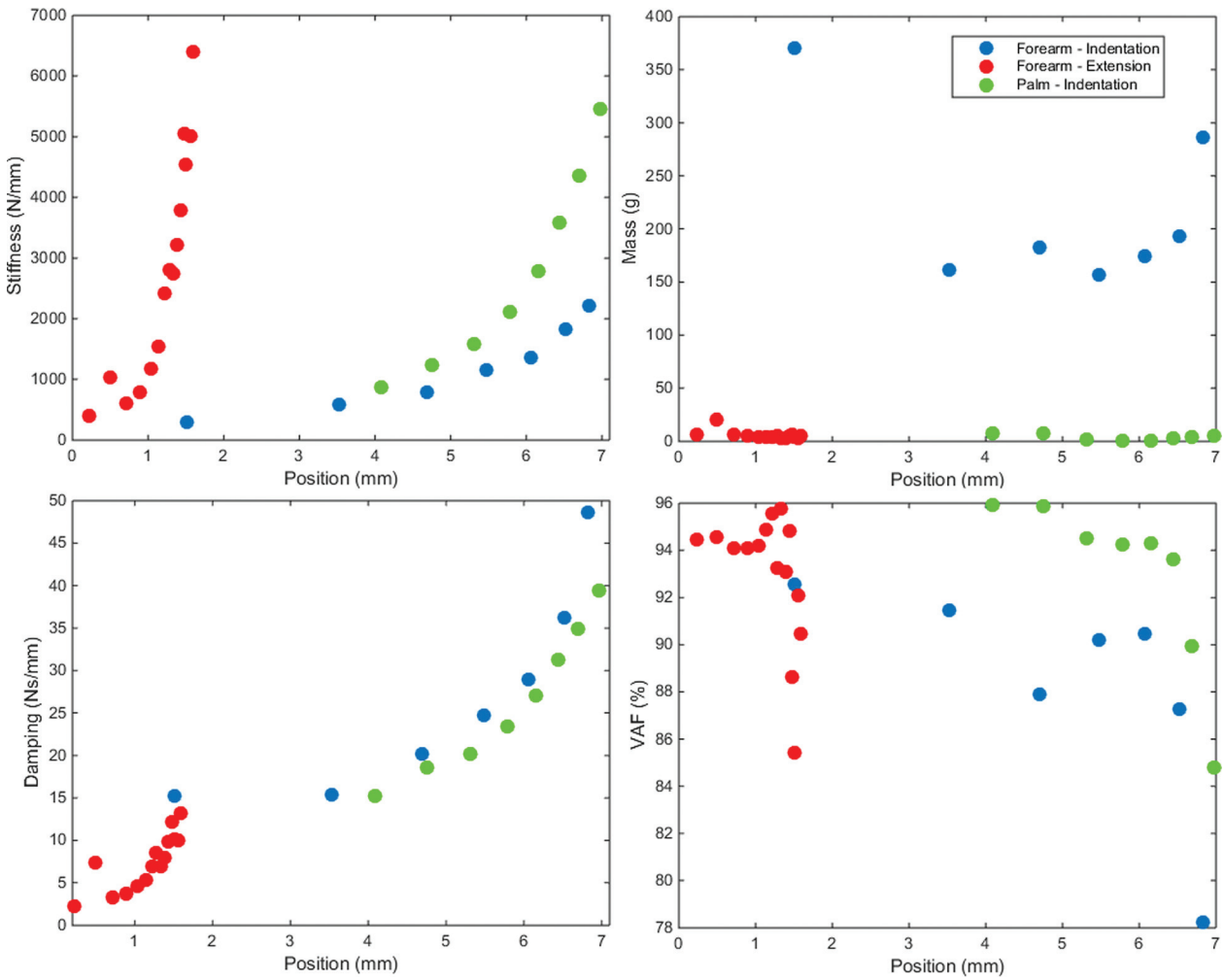

Fig. 8 Representative experimental results from linear incremental stochastic system identification of a volar forearm and thenar eminence test are shown. Each plot shows a different linear output property as produced by an incremental loading scheme, in different perturbation directions and/or sites. (*a*) The tissue stiffness estimated at various stretches is shown. (*b*) The perturbed mass estimated at various stretches is shown, after the actuator mass is subtracted. (*c*) The tissue damping at various stretches is shown, after the actuator damping is subtracted. (*d*) The VAF for each site is plotted against actuator tip position.

extension test on the forearm in Fig. 8. Parameter estimates were made using protocol B (triangle wave preconditioning). The general trends seen in the mass, stiffness, damping, and VAF when plotted against position were consistent over all the five subjects tested.

Discussion

This paper presents a method for characterizing in vivo the multidirectional dynamic properties of skin using one device in a single configuration. Development and modifications to the hardware, electronics, and software of an existing multi-axis microrobot are detailed. Linear dynamic and Wiener static nonlinear stochastic system identification protocols have been adapted to a device that is more versatile than those used in previous dynamic skin studies [21,23,24,30–35]. Stochastic system identification was applied to the volar forearm and thenar eminence, the latter being a location for which there was little dynamic data.

Identifying the nonlinear, viscoelastic, and anisotropic properties of skin in vivo is important for the diagnosis and treatment of conditions that affect its mechanical properties. In the present studies, the probe tip was attached to the skin via cyanoacrylate, which provided a secure but flexible connection. If studies are extended to perturb more sensitive skin, a solvent may be introduced to gently remove the cyanoacrylate after test completion.

Wiener systems have been shown to produce good fits to dynamic skin behavior [25,27]. Although other nonlinear stochastic models, such as Hammerstein and Volterra kernels, have been applied to human tissue, Wiener models have the highest VAF in skin [24]. In this study, linear models accounted for 85–93% of the variance. The incorporation of Wiener nonlinearities into the model increased the VAF to between 94% and 97%. Previous studies have reported linear VAF between 75% and 81% and an increase in the VAF of around 5% when Wiener models were added. The relatively high VAF with linear models in the present experiment may be an artefact of the stroke length of the device used to perturb the skin. Although the current device did not produce deformations as large as those implemented by Chen and Hunter [27] and Sandford et al. [20], the increase in VAF with the Wiener model shows that nonlinearities in the parameters are nevertheless evident in the results.

The use of stochastic system identification techniques with the microrobot provided a rapid means of characterizing skin properties. This should not have impacted any of the measurements made. Parameters were identified from 5 s samples, and the whole test procedure for full-scale perturbations lasted under 2 min per direction. Rapid testing procedures are of benefit in many applications, such as assessing the efficacy of skin care products or providing a relatively quick means of assessing the condition of the skin in a dehydrated patient in a clinic.

A limitation of the current device was evident when attempting to perform extension tests in multiple directions. In most subjects, extensions on the palm in directions 1 and 2 could not be analyzed, as the system applied insufficient force to deform the skin. Glabrous skin has previously been shown to be significantly stiffer than hairy skin [20]. In this study, the force was limited by the power supply and current amplifiers, which led to degradation in the stochastic input signal above the range of forces used. The power supply and amplifiers were originally chosen for lower frequency perturbations, and a purpose-built setup may allow future multidirectional characterization of stiffer tissues such as those on the palm. Additionally, the relatively large estimates of perturbed mass in extension directions raise concerns about the values reported. These values represent approximately 11–21% of the robot's moving mass and therefore may not be reliable. A lighter probe tip may facilitate more reliable measurements of mass in extension.

This paper provides new measures of the dynamic properties of the skin of the thenar eminence. Previous studies of the mechanical properties of skin on the palm have used suction [36], ballistometry [36], and optical coherence elastography [32,37]. Liang and Boppart [32] reported a Young's modulus of 24.9 kPa for the thenar eminence, compared to 101.18 kPa for the volar forearm, and Li et al. reported separate Young's moduli for the dermis (250 kPa) and subcutaneous fat (50 kPa) of the palm [37]. Although Young's moduli do not capture the anisotropic, viscoelastic, and nonlinear properties of skin, it is commonly used in the literature and provides one means of comparing deformation studies. It is important to note that changes in the mechanical properties of skin with disease or as a consequence of treatment methodologies may be identified through system identification parameters, rather than simple parameters such as Young's moduli.

The Poisson's ratio for skin is approximately 0.45 [38]. Using Eq. (3) and the incremental estimates in our study provide a Young's modulus of 63 kPa at small indentation depths and 460 kPa at greater depths on the forearm and 170 kPa to 1090 kPa for the palm. Neo-Hookean parameters derived from Eq. (4) were $c_{10} = 11$ kPa and $D_1 = 0.0095$ for small indentation depths and $c_{10} = 79$ kPa and $D_1 = 0.0013$ at greater depths on the forearm. In the thenar eminence, neo-Hookean parameters increased from $c_{10} = 29$ kPa and $D_1 = 0.0035$, to $c_{10} = 188$ kPa and $D_1 = 0.0005$. The c_{10} parameters at low displacements lie within those reported for in vivo skin under suction by Hendriks et al. [39], while the upper displacement parameters are similar to the values described by Tran et al. under indentation [40]. This model has been shown to capture some of the nonlinearity of in vivo skin, but often fails to capture the degree of nonlinearity, and ignores viscoelastic and anisotropic behavior. More complex mechanical models such as the Ogden, Gasser–Ogden–Holzapfel, and Tong and Fung constitutive models have shown better fits to skin. However, these require complex finite-element formulations to interpret the experimental results, and nonlinear optimization of parameter sets, which are time-consuming and raise questions of parameter identifiability due to the large number of parameters. A simpler model, such as the Wiener system, may therefore provide a more clinically friendly option at present, due to the relatively few parameters calculated and rapid identification. While the identified mechanical properties are consistent with existing literature, the range in previously reported properties may be partly due to differences in test procedures. In the future, the parameters identified through Wiener static nonlinearity approaches should be compared to those found using the same sample.

The parameter values suggest that, at small indentations, perturbations were mostly made to the more compliant layers. The initial response could be an isolated response from the hypodermis, as the early incremental estimates match reported moduli for subcutaneous fat [37], with the increasing stiffness caused by the gradual recruitment of the living epidermis, dermis, stratum corneum, and eventually the underlying muscle. The much higher stiffness of the thenar eminence is likely due to its relatively thick epidermis, which has previously been reported to be around 1 MPa [41]. The stratum corneum in glabrous skin ranges from approximately 100 μm to 200 μm, as compared to 10 μm to 40 μm in hairy skin. Identifying Wiener nonlinearities or measuring the incremental moduli may provide a means of characterizing the thickness of skin layers. If the change in modulus with indenter depth is shown to correlate with the recruitment of various skin layers, this information could be useful in specifying a velocity profile for delivering a drug to a specific depth in the skin for site-specific action [42]. For example, many compounds are designed for subcutaneous delivery and must penetrate the dermis while avoiding underlying tissues. Accurate delivery requires knowledge of local mechanical properties and layer thickness. Thus, controlled delivery of such drugs will require rapid soft tissue characterization immediately prior to injection.

The range in Young's moduli and neo-Hookean parameters found at full-scale characterization and at different incremental loads fits well with existing literature, in both normal and tangential deformation modes. While some indentation devices have

reported much lower stiffness on the forearm (approximately 8 kPa) [8,10], these estimates have been generated at much lower strains. Other deformation profiles report higher values. Estimates from torsion experiments have ranged from 20 kPa to 100 kPa [43], to moduli over 1 MPa on the forearm [6]. Suction tests have also resulted in considerable variability in Young's moduli from as low as 130 kPa to as high as 57 MPa [44].

Khatyr et al. [45] reported extensometer-derived Young's moduli values of 130 kPa to 660 kPa, depending on the direction of extension. These tests most closely resemble the lateral stretches in the present study. In the former study, it was found that the average elastic modulus along the axis of the arm was approximately five times higher than its modulus in the perpendicular direction, and twice as high as that at 135 deg from the axis [45]. The present findings show a lower degree of anisotropy; the maximum stiffness and Young's modulus seen in direction 1 (Fig. 4) align most closely with the long axis of the forearm. Flynn et al. [28] demonstrated that although the proximal–distal axis of the arm produced the stiffest response, the perpendicular direction did not produce the least stiff response, which was found at 60 deg from the long axis. Likewise, we found the lowest modulus in direction 2, rather than the approximately perpendicular orientation of direction 3 relative to the long axis of the arm. These results are consistent with Langer's lines on the anterior forearm [46], where the lines in the test area deviate from the long axis of the arm and align more closely with direction 1.

The within-subject CVs of the Wiener static nonlinearity parameters provide insight into the reliability of the device. With normal indentation, the microrobot produced CVs ranging between 2% and 11%. The performance for extension tests was less reliable, with CVs ranging from 2% to 19%. However, the CV within individuals under extension is still within the ranges reported for commercial devices, such as the Cutometer and Reviscometer (6–14% [47]), Dermaflex (11–35% [36]), and DiaStron (2–17% [36]). The CVs for scaled mass and scaled damping remained low across all the experimental modes and locations (2–4% normal and 2–6% extension), and the CV for the compressible depth parameter was less than 11% across tests. Improvements in the CVs of measurements made during extension may occur by increasing the force input, thereby increasing the signal-to-noise ratio of the impulse response function. The microrobot compares favorably with existing commercial devices used to assess the skin's properties. The reliability of the microrobot in measuring the skin's mechanical properties in multiple directions suggests that it could be a useful measurement tool for assessing conditions such as skin hydration and wound healing. It also holds promise for testing the efficacy of skincare products, particularly those that contain high-molecular weight polymers used to induce skin tightness [20]. In future studies, force transducers may be added to the mount, or probe tip, of the microrobot, which will allow precise control of the initial normal force of the probe on the skin and may reduce CVs.

This paper presents a unique study of the effects of preconditioning modes on incremental system identification. The incremental law of skin was presented over 30 years ago [48], but has received relatively little attention since then. Under quasi-static loading, the stress–strain plots of skin have been shown to vary with the scale of the perturbation. Stress–strain plots taken from small perturbations with incrementing displacements have shown locally linear responses, where the slope does not equate to the tangent of the loading, unloading, or mean curve of the entire stress–strain response. This study is unique in that it demonstrates that the effect holds under dynamic loading, in both indentation and extension experiments. It demonstrates that the depth- or stretch-dependent damping and stiffness that occurs from strain-hardening occurs in both glabrous and hairy skin and indicates higher stiffness at local perturbations, as seen in the flatter slopes of the incremental loading curves. The selection of a triangular wave or average incremental force preconditioning regime made no clear difference to the estimation of skin parameters. What is more important is providing sufficient preconditioning throughout the entire test range. The results suggest that large-scale preconditioning of the skin does not adequately condition the skin at the smaller scale, so incremental measures must be made with their own tailored preconditioning scheme. Although incremental measures use linear system identification to provide simpler mathematical means of characterizing the nonlinear response of skin, they come at the cost of lengthy experiments, and the results are more difficult to compare across subjects.

The reduction in the VAF for increments at the upper limits is likely due to the reduced signal-to-noise ratio as the increased stiffness at high extension reduces the resulting displacement. Outliers are seen in one set of results, at approximately 0.5 mm extension in the mass, stiffness, and damping terms. This may be due to the significantly shorter duration of tests at each increment in comparison to the full-scale tests.

The microrobot and associated analytic techniques provide a unique system to mechanically analyze the nonlinear, anisotropic, viscoelastic, and heterogeneous properties of skin. It is the first device to employ stochastic system identification approaches in multiple directions without the need to reconfigure or reposition the probe relative to the skin. The results demonstrate its ability to measure skin properties in an expedient and reliable manner. The linear parameter values that were measured for skin lie within the ranges reported previously using a variety of techniques, and the Wiener parameters are comparable to those presented in previous studies using stochastic system identification. The versatility, reliability, and speed at which the microrobot device quantitatively measures the properties of skin underscore its potential usefulness in clinical research.

Acknowledgment

The authors would like to thank Dr. E. Chen for her expertise on stochastic system identification, Dr. C. Flynn for his help with microrobotics, and S. Olding for his help in device manufacturing.

This work was supported in part by the New Zealand Foundation for Research, Science and Technology, through Grant Nos. NERF UOA21647.001 and NERF 9077/3608892, and by the Medical Technologies Centre of Research Excellence (MedTech CoRE), funded by the Tertiary Education Commission of New Zealand.

Nomenclature

B = damping parameter of linear system
B_s = scaled mass parameter of Wiener system
C_1 = compressible thickness parameter of Wiener system
C_2 = degree of nonlinearity parameter of Wiener system
C_{10} = neo-Hookean parameter
CV = coefficient of variation
D_1 = neo-Hookean parameter
E = Young's modulus
K = stiffness parameter of linear system
M = mass parameter of linear system
M_s = scaled mass parameter of Wiener system
VAF = variance accounted for
ν = Poisson's ratio

References

[1] Hendriks, F. M., Brokken, D., Oomens, C. W. J., Bader, D. L., and Baaijens, F. P. T., 2006, "The Relative Contributions of Different Skin Layers to the Mechanical Behavior of Human Skin In Vivo Using Suction Experiments," Med. Eng. Phys., **28**(3), pp. 259–266.

[2] Delalleau, A., Josse, G., Lagarde, J.-M., Zahouani, H., and Bergheau, J.-M., 2008, "A Nonlinear Elastic Behavior to Identify the Mechanical Parameters of Human Skin In Vivo," Skin Res. Technol., **14**(2), pp. 152–164.

[3] Delalleau, A., Josse, G., George, J., Yassine, M., Ossant, F., and Lagarde, J.-M., 2009, "A Human Skin Ultrasonic Imaging to Analyse Its Mechanical Properties," Eur. J. Comput. Mech., **18**(1), pp. 105–116.

[4] Krueger, N., Luebberding, S., Oltmer, M., Streker, M., and Kerscher, M., 2011, "Age-Related Changes in Skin Mechanical Properties: A Quantitative Evaluation of 120 Female Subjects," Skin Res. Technol., **17**(2), pp. 141–148.

[5] Sutradhar, A., and Miller, M. J., 2012, "In Vivo Measurement of Breast Skin Elasticity and Breast Skin Thickness," Skin Res. Technol., (11), pp. 1–9.
[6] Escoffier, C., de Rigal, J., Rochefort, A., Vasselet, R., Leveque, J. L., and Agache, P., 1989, "Age-Related Mechanical Properties of Human Skin: An In Vivo Study," J. Invest. Dermatol., **93**(3), pp. 353–357.
[7] Leveque, J. L., Corcuff, P., de Rigal, J., and Agache, P., 1984, "In Vivo Studies of the Evolution of Physical Properties of the Human Skin With Age," Int. J. Dermatol., **23**(5), pp. 322–329.
[8] Zahouani, H., Pailler-Mattei, C., Sohm, B., Vargiolu, R., Cenizo, V., and Debret, R., 2009, "Characterization of the Mechanical Properties of a Dermal Equivalent Compared With Human Skin In Vivo by Indentation and Static Friction Tests," Skin Res. Technol., **15**(1), pp. 68–76.
[9] Flynn, C., Taberner, A. J., Nielsen, P. M. F., and Fels, S., 2013, "Simulating the Three-Dimensional Deformation of In Vivo Facial Skin," J. Mech. Behav. Biomed. Mater., **28**, pp. 484–494.
[10] Pailler-Mattéi, C., Bec, S., and Zahouani, H., 2008, "In Vivo Measurements of the Elastic Mechanical Properties of Human Skin by Indentation Tests," Med. Eng. Phys., **30**(5), pp. 599–606.
[11] Delalleau, A., Josse, G., Lagarde, J. M., Zahouani, H., and Bergheau, J. M., 2008, "Characterization of the Mechanical Properties of Skin by Inverse Analysis Combined With an Extensometry Test," Wear, **264**(5–6), pp. 405–410.
[12] Woo, M. S., Moon, K. J., Jung, H. Y., Park, S. R., Moon, T. K., Kim, N. S., and Lee, B. C., 2014, "Comparison of Skin Elasticity Test Results From the Ballistometer® and Cutometer®," Skin Res. Technol., **20**(4), pp. 422–428.
[13] Sandrin, L., Tanter, M., Gennisson, J.-L., Catheline, S., and Fink, M., 2002, "Shear Elasticity Probe for Soft Tissues With 1-D Transient Elastography," IEEE Trans. Ultrason. Ferroelectr. Freq. Control, **49**(4), pp. 436–446.
[14] Zhang, X., and Greenleaf, J. F., 2007, "Estimation of Tissue's Elasticity With Surface Wave Speed," J. Acoust. Soc. Am., **122**(5), pp. 2522–2525.
[15] Verhaegen, P. D. H. M., Res, E. M., van Engelen, A., Middelkoop, E., and van Zuijlen, P. P. M., 2010, "A Reliable, Non-Invasive Measurement Tool for Anisotropy in Normal Skin and Scar Tissue," Skin Res. Technol., **16**(3), pp. 325–331.
[16] Coutts, L., Bamber, J., and Miller, N., 2013, "Multi-Directional In Vivo Tensile Skin Stiffness Measurement for the Design of a Reproducible Tensile Strain Elastography Protocol," Skin Res. Technol., **19**(1), pp. 37–44.
[17] Lim, K. H., Chew, C. M., Chen, P. C. Y., Jeyapalina, S., Ho, H. N., Rappel, J. K., and Lim, B. H., 2008, "New Extensometer to Measure In Vivo Uniaxial Mechanical Properties of Human Skin," J. Biomech., **41**(5), pp. 931–936.
[18] Jacquet, E., Josse, G., Khatyr, F., and Garcin, C., 2008, "A New Experimental Method for Measuring Skin's Natural Tension," Skin Res. Technol., **14**(1), pp. 1–7.
[19] Diridollou, S., Berson, M., Vabre, V., Black, D., Karlsson, B., Auriol, F., Gregoire, J. M., Yvon, C., Vaillant, L., Gall, Y., and Patat, F., 1998, "An In Vivo Method for Measuring the Mechanical Properties of the Skin Using Ultrasound," Ultrasound Med. Biol., **24**(2), pp. 215–224.
[20] Sandford, E., Chen, Y., Hunter, I., Hillebrand, G., and Jones, L., 2012, "Capturing Skin Properties From Dynamic Mechanical Analyses," Skin Res. Technol., **19**(1), pp. e339–48.
[21] Kennedy, B. F., Hillman, T. R., McLaughlin, R. A., Quirk, B. C., and Sampson, D. D., 2009, "In Vivo Dynamic Optical Coherence Elastography Using a Ring Actuator," Opt. Express, **17**(24), pp. 21762–21772.
[22] Boyer, G., Zahouani, H., Le Bot, A., and Laquieze, L., 2007, "In Vivo Characterization of Viscoelastic Properties of Human Skin Using Dynamic Micro-Indentation," 29th Annual International Conference of the IEEE Engineering in Medicine and Biology Society (EMBS 2007), Lyon, France, Aug. 22–26, pp. 4584–4587.
[23] Boyer, G., Laquièze, L., Le Bot, A., Laquièze, S., and Zahouani, H., 2009, "Dynamic Indentation on Human Skin In Vivo: Ageing Effects," Skin Res. Technol., **15**(1), pp. 55–67.
[24] Chen, Y., and Hunter, I. W., 2013, "Nonlinear Stochastic System Identification of Skin Using Volterra Kernels," Ann. Biomed. Eng., **41**(4), pp. 847–862.
[25] Chen, Y., and Hunter, I. W., 2012, "Stochastic System Identification of Skin Properties: Linear and Wiener Static Nonlinear Methods," Ann. Biomed. Eng., **40**(10), pp. 2277–2291.
[26] Holzapfel, G. A., and Ogden, R. W., 2008, "On Planar Biaxial Tests for Anisotropic Nonlinearly Elastic Solids. A Continuum Mechanical Framework," Math. Mech. Solids, **14**(5), pp. 474–489.
[27] Chen, Y., and Hunter, I. W., 2009, "In Vivo Characterization of Skin Using a Weiner Nonlinear Stochastic System Identification Method," Annual International Conference of the IEEE Engineering in Medicine and Biology Society (EMBC 2009), Minneapolis, MN, Sept. 3–6, pp. 6010–6013.
[28] Flynn, C., Taberner, A., and Nielsen, P., 2011, "Mechanical Characterisation of In Vivo Human Skin Using a 3D Force-Sensitive Micro-Robot and Finite Element Analysis," Biomech. Model. Mechanobiol., **10**(1), pp. 27–38.
[29] Flynn, C., Taberner, A., and Nielsen, P., 2011, "Measurement of the Force–Displacement Response of In Vivo Human Skin Under a Rich Set of Deformations," Med. Eng. Phys., **33**(5), pp. 610–619.
[30] Sandford, E., Chen, Y., Hunter, I., Hillebrand, G., and Jones, L., 2013, "Capturing Skin Properties From Dynamic Mechanical Analyses," Skin Res. Technol., **19**(1), pp. e339–e348.
[31] Finlay, B., 1970, "Dynamic Mechanical Testing of Human Skin "In Vivo," J. Biomech., **3**(6), pp. 557–568.
[32] Liang, X., and Boppart, S. A., 2010, "Biomechanical Properties of In Vivo Human Skin From Dynamic Optical Coherence Elastography," IEEE Trans. Biomed. Eng., **57**(4), pp. 953–959.
[33] Kearney, S. P., Khan, A., Dai, Z., and Royston, T. J., 2015, "Dynamic Viscoelastic Models of Human Skin Using Optical Elastography," Phys. Med. Biol., **60**(17), pp. 6975–6990.
[34] Khatyr, F., and Imberdis, C., 2004, "Model of the Viscoelastic Behaviour of Skin In Vivo and Study of Anisotropy," Skin Res. Technol., **10**(2), pp. 96–103.
[35] Weickenmeier, J., Jabareen, M., and Mazza, E., 2015, "Suction Based Mechanical Characterization of Superficial Facial Soft Tissues," J. Biomech., **48**(16), pp. 4279–4286.
[36] Jemec, G. B. E., Selvaag, E., Agren, M., and Wulf, H. C., 2001, "Measurement of the Mechanical Properties of Skin With Ballistometer and Suction Cup," Skin Res. Technol., **7**(2), pp. 122–126.
[37] Li, C., Guan, G., Reif, R., Huang, Z., and Wang, R. K., 2012, "Determining Elastic Properties of Skin by Measuring Surface Waves From an Impulse Mechanical Stimulus Using Phase-Sensitive Optical Coherence Tomography," J. R. Soc. Interface, **9**(70), pp. 831–841.
[38] Raveh Tilleman, T., Tilleman, M. M., and Neumann, M. H. A., 2004, "The Elastic Properties of Cancerous Skin: Poisson's Ratio and Young's Modulus," Isreal Med. Assoc. J., **6**(12), pp. 753–755.
[39] Hendriks, F. M., Brokken, D., van Eemeren, J. T. W. M., Oomens, C. W. J., Baaijens, F. P. T., and Horsten, J. B. A. M., 2003, "A Numerical–Experimental Method to Characterize the Non-Linear Mechanical Behaviour of Human Skin," Skin Res. Technol., **9**(3), pp. 274–283.
[40] Tran, H. V., Charleux, F., Rachik, M., Ehrlacher, A., and Ho Ba Tho, M. C., 2007, "In Vivo Characterization of the Mechanical Properties of Human Skin Derived From MRI and Indentation Techniques," Comput. Methods Biomech. Biomed. Eng., **10**(6), pp. 401–407.
[41] Geerligs, M., van Breemen, L., Peters, G., Ackermans, P., Baaijens, F., and Oomens, C., 2011, "In Vitro Indentation to Determine the Mechanical Properties of Epidermis," J. Biomech., **44**(6), pp. 1176–1181.
[42] Hatefi, A., and Amsden, B., 2002, "Biodegradable Injectable In Situ Forming Drug Delivery Systems," J. Controlled Release, **80**(1–3), pp. 9–28.
[43] Sanders, R., 1973, "Torsional Elasticity of Human Skin In Vivo," Pflugers Arch., **342**(3), pp. 255–260.
[44] Grahame, R., and Holt, P. J. L., 1969, "The Influence of Ageing on the In Vivo Elasticity of Human Skin," Gerontology, **15**(2–3), pp. 121–139.
[45] Khatyr, F., Imberdis, C., Vescovo, P., Varchon, D., and Lagarde, J.-M., 2004, "Model of the Viscoelastic Behaviour of Skin In Vivo and Study of Anisotropy," Skin Res. Technol., **10**(2), pp. 96–103.
[46] Langer, K., 1978, "On the Anatomy and Physiology of the Skin—I: The Cleavability of the Cutis," Br. J. Plast. Surg., **31**(1), pp. 3–8.
[47] Nizet, J. L., Piérard-Franchimont, C., and Piérard, G. E., 2001, "Influence of Body Posture and Gravitational Forces on Shear Wave Propagation in the Skin," Dermatology, **202**(2), pp. 177–180.
[48] Fung, Y., 1993, *Biomechanics: Mechanical Properties of Living Tissues*, Springer-Verlag, New York.